ACS OMEGA

http://pubs.acs.org/journal/acsodf

Article

Characteristics and the Model of Thermal Evolution and Gas Generation of Late Paleozoic Coal in the Qinshui Basin, Based on Hydrous Pyrolysis

Ruilin Hao, Wenhui Huang,* and Bo Jiu

Cite This: *ACS Omega* 2021, 6, 17660−17673

Read Online

ACCESS | Metrics & More | Article Recommendations

ABSTRACT: The Qinshui basin is an important coal-accumulating basin in China, and its Late Paleozoic coal is an important source rock of coalbed methane in the basin. Its thermal evolution and gas generation characteristics determined the grade of coalbed methane resources, especially the coal measure free gas resources in the basin. Late Paleozoic coal samples were collected for organic geochemical analysis, a high-volatile bituminous coal was used for hydrous pyrolysis, to propose the thermal evolution characteristics, gas generation characteristics, thermal evolution, and free gas accumulation model, and the Ordos Basin is compared. The results show that the variation trends of various geochemical parameters are different with the increase in R_o. Hydrous pyrolysis shows that the gas production potential of coal is excellent. The gases produced consist mainly of CH_4, C_{2-}, CO_2, and H_2. C_{2-} is produced only before the simulated temperature of 550 °C, and oil is produced only before the temperature of 500 °C. The thermal evolution stages can be divided into the immature stage, symbiosis stage, wet gas stage, and dry gas stage, and the symbiosis stage can be divided into the preliminary stage and mainly gas stage. R_o, T_{max}, (2+3)MP/(1+9)MP, saturated+arene, V_{daf}, and H/C can be used as indicators of the thermal evolution stages. On the plane, the distribution of thermal evolution stages of the Shanxi Formation and the Taiyuan Formation is very alike. The gas generating strength of the Taiyuan Formation is higher than that of the Shanxi Formation. The gas generating strength in the north of the Taiyuan Formation is higher, while that in the south of the Shanxi Formation is higher. The second gas generation stage has a good spatio-temporal configuration relationship with accumulation factors, and the gas production is large, which is beneficial to the enrichment of the coal measure free gas resources. Relatively, the Ordos Basin has better prospects for exploration and development.

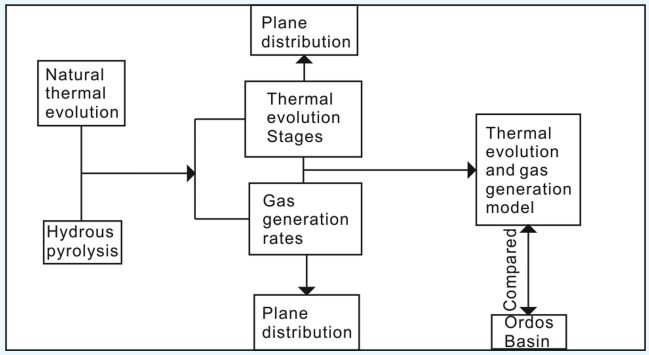

1. INTRODUCTION

With the increasing demand for energy in the world, the research on unconventional oil and gas resources has been paid more and more attention globally, and their exploration and development process has also made great progress in the United States,[1,2] China,[3] Canada,[4,5] and other places.[6,7] In China, unconventional oil and gas resources such as coalbed methane, shale gas, and tight gas have been studied and developed for decades, and breakthroughs have been made in the Qinshui Basin,[8−10] Ordos Basin,[11,12] Sichuan Basin,[13,14] and other places.[15−17] The Qinshui Basin is one of the important coal-accumulating basins in China. The coal seams in the basin are widely distributed with large thicknesses, and the coal reserves are abundant.[18] In the coal measure strata, there are many dark mudstone or shale distributions and carbonate strata rich in organic matter,[19,20] providing excellent source rock conditions for coalbed methane, tight gas, and shale gas in the basin. Also, because of the maturity and wide application of hydraulic fracturing technology, the unconventional oil and gas resources in the Qinshui Basin have a good prospect of exploration and development.[21,22]

In the Qinshui Basin, coalbed methane is the most important unconventional gas resource. It has a wide distribution, a large number of resources, and a high resource abundance,[23,24] and the dominant strata are the coal-bearing strata of the Late Paleozoic Carboniferous Taiyuan Formation and Permian Shanxi Formation.[25] Therefore, the thermal evolution characteristics, hydrocarbon generation characteristics of coal, and their relationship can be well-studied through the data of the Qinshui Basin. However, the coal-bearing strata in the Late Paleozoic underwent a complex temperature and pressure evolution,[26] and

Received: April 27, 2021
Accepted: June 17, 2021
Published: July 1, 2021

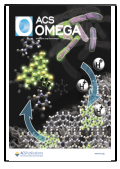

https://doi.org/10.1021/acsomega.1c02211
ACS Omega 2021, 6, 17660−17673

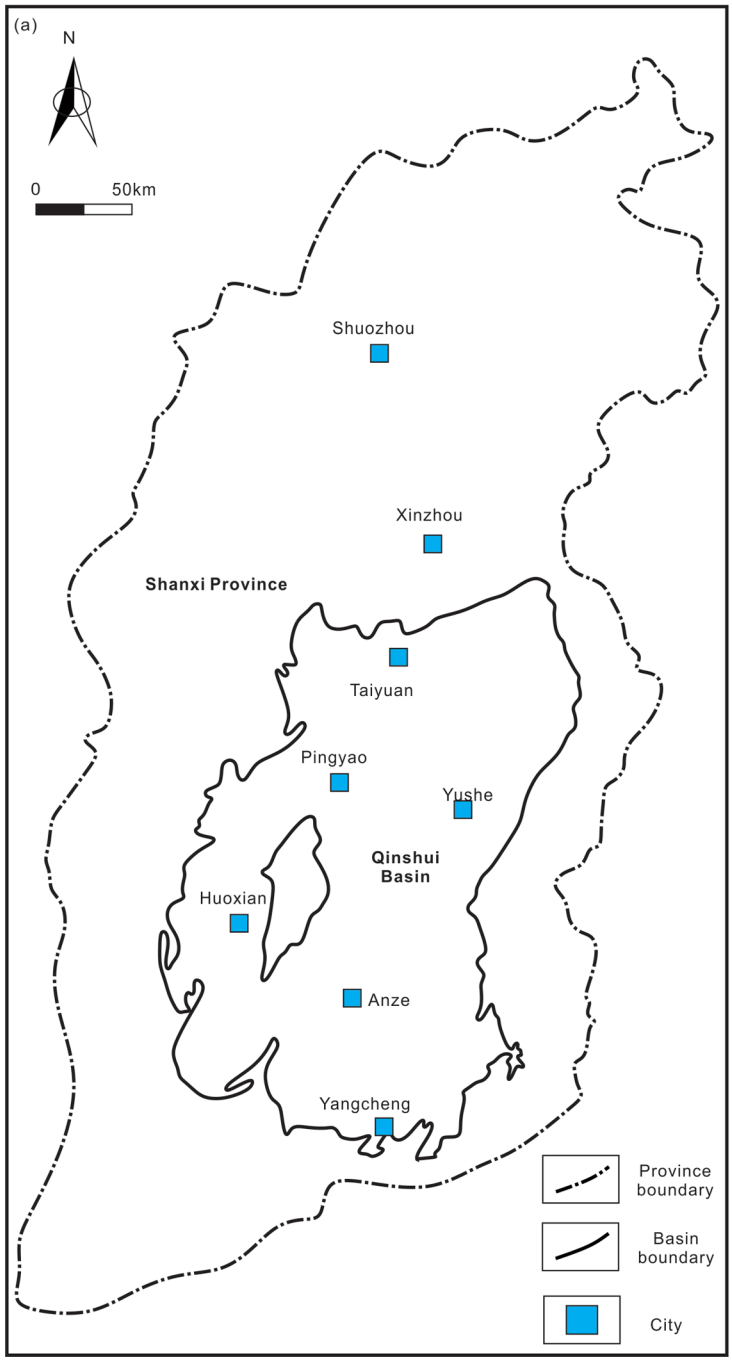

(b) System	Series	Formation	Markers for the whole Shanxi Province: Name	Code
Permian	Upper Permian	Shiqianfeng		
			K_8 Sandstone	K_8
		Shangshihezi	Siliceous rocks (chert)	G_s
	Middle Permian		K_6 Sandstone	K_6
		Xiashihezi	Taohua Mudstone	T_h
			Luotuobozi Sandstone	K_4
	Lower Permian	Shanxi	Upper coal Measures	C_s
			Beichagou Sandstone	K_3
		Taiyuan	Shangou Limestone	L_6
			Fucheng Limestone	Upper L_5
			Dongdayao Limestone	L_5
			Qiligou Sandstone	Q_s
			Xiedao Limestone	L_4
			Maoergou Limestone	L_3, L_2
			Miaogou Limestone	L_1
Carboniferous	Upper Carboniferous		Lower coal Measures	C_x
			Wujiayu Limestone	L_0
			Jinci Sandstone	K_1
		Benxi	Bangou Limestone	L_b
			Fe-Al bearing Mudstone	Tl

Figure 1. Location map and stratigraphic subdivision of the Qinshui Basin: (a) location map; (b) stratigraphic subdivision (modified from ref 42). Reprinted (Adapted or Reprinted in part) from ref 42.

the coal metamorphism was generally high, so it was difficult to intuitively study the thermal evolution characteristics and hydrocarbon generation characteristics of coal. Targeted at the thermal evolution characteristics of the basin, predecessors used the apatite fission track method and the advanced Schlumberger PetroMod software, to provide detailed information about variations in the geothermal field and some geochemical characteristics of the coal, and proposed the tectono-thermal evolution model.[26,27] Targeted at the gas generation characteristics, predecessors used the results of pyrolysis of peat or coal to determine the lumped kinetics parameters[28] and the advanced Schlumberger PetroMod software, to propose the gas generation history.[26,29] Also, the accumulation model of coalbed methane was pointed out.[30]

However, these studies mainly focus on the tectono-thermal evolution, but the characteristics and indexes of coal thermal evolution stages are not clearly understood. Also, these studies have not proposed the gas generation rate at different vitrinite reflectance (R_o), the gas generating strength, and its plane distribution characteristics and have not gotten the relationship between the accumulation events of the coal measure free gas. Therefore, a large number of geochemical experiments were carried out on the Late Paleozoic coals with different degrees of thermal evolution in the Qinshui Basin, and hydrous pyrolysis was carried out on the high-volatile bituminous coal[31] in the

https://doi.org/10.1021/acsomega.1c02211
ACS Omega 2021, 6, 17660−17673

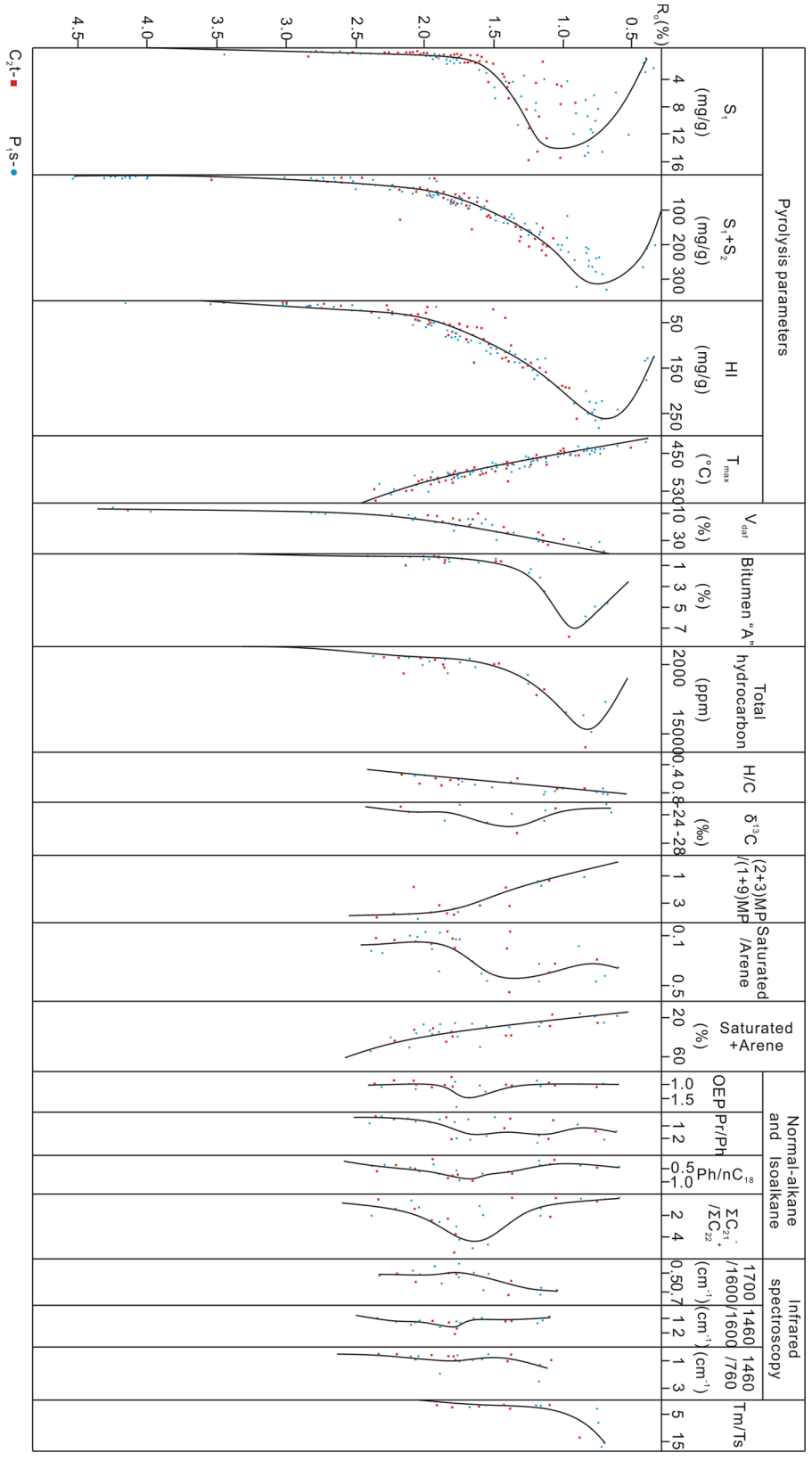

Figure 2. Natural thermal evolution profile of the Late Paleozoic coal in the Qinshui Basin.

Qinshui Basin to analyze the yield and geochemical characteristics of the products in each stage. According to the change characteristics of geochemical parameters and the characteristics of hydrous pyrolysis products, the thermal evolution stages of coal are divided, and the characteristics of each stage, the classification indexes, and the plane distribution characteristics are pointed out. Combining the gas production in hydrous pyrolysis and the previous research results, the gas generation rate at different R_o is obtained, the gas generating strength is calculated, and the characteristics of gas generating strength in

https://doi.org/10.1021/acsomega.1c02211
ACS Omega 2021, 6, 17660−17673

the plane are pointed out. Combining the results, tectonic and sedimentary events of the basin, the thermal evolution, and the free gas accumulation model in the basin are pointed out. Finally, the similarities and differences between the Qinshui Basin and the Ordos Basin are compared based on the previous research results, which is beneficial to guide further exploration and development.

2. GEOLOGICAL SETTING

The Qinshui Basin is located in the southeast of the Shanxi Province, covering an area of about 26,000 km^2 (Figure 1). It is rich in coal and coalbed methane resources, and it is the only large basin in China to develop coalbed methane on an industrial scale.[32−34] Structurally, it is located in the central part of the North China Craton and is generally a large-scale complex syncline with axial NNE−SSW.[35,36] After a series of tectonic influence, especially during the Yanshanian and the Himalayan period, the Qinshui basin formed a complex structural setting.[37−41]

After a series of tectonics and discontinuous deposition, the Qinshui Basin became a residual structural basin with a thickness of 200−3000 m of coal-bearing strata,[26] and under the influence of intermittent uplift and subsidence, multiple periods of transgression occurred in the early and late Carboniferous and early Permian, resulting in obvious regional cycles of coal seams, carbonate rocks, mudstones, and sandstone in the sedimentary strata from the Taiyuan Formation to the Shanxi Formation[43−47] (Figure 1). Due to the large scope of the basin, the names of coal seams and main marker beds in different areas of the basin are different. The boundaries of the Benxi and the Taiyuan Formation, the Taiyuan and the Shanxi Formation, the Shanxi and the Xiashihezi Formation are Jinci Sandstone (K_1) and Bangou Limestone (L_b), Beichagou Sandstone (K_3) and Shangou Limestone (L_6), and Luotuobozi Sandstone (K_4) and Upper coal measures (C_s), respectively.[42] There are two main coal measures, the Lower coal measures (including the no. 15 coal) in the Taiyuan Formation and the Upper coal measures (including the no. 3 coal) in the Shanxi Formation. The no. 15 and no. 3 coals are regionally stable and mainly minerable.[42] The thickness of no. 15 coal is 0.21−9.87 m, and the average is 3.26 m.[44] The maximum vitrinite reflectance ($R_{o,max}$) of no.15 coal is 2.13−4.25%,and the average is 3.14%.[44] The thickness of no. 3 coal is 2.75−7.10 m, and the $R_{o,max}$ is 3.25−4.05%.[18]

The source rocks of the Late Paleozoic coal measure free gas reservoirs are mainly coal and dark mudstone of the Taiyuan Formation and the Shanxi Formation. The kerogen type of coal is mainly type III, while the dark mudstone or shale is mainly type III, and part of it is Type II_2.[19,48] The hydrocarbon generation capacity of coal is much greater than those of dark mudstone and shale, which is the most important source rock.[49−51]

3. RESULTS

3.1. Natural Thermal Evolution Characteristics. From the characteristics of natural thermal evolution (Figure 2), it can be seen that the parameter curves of the Taiyuan Formation and the Shanxi Formation are not very consistent, and the R_o of coal samples from the Taiyuan Formation is basically greater than 1.0. However, in terms of the overall change trend, the Taiyuan Formation and the Shanxi Formation are relatively similar.

1. The contents of S_1, (S_1+S_2), HI, bitumen "A", and total hydrocarbons increase first and then decrease with the increase in R_o. These five parameters reach their maximum value when R_o is 0.7−1.3%. Subsequently, the parameters gradually decrease. After R_o > 1.0%, (S_1+S_2), HI, bitumen "A", and total hydrocarbons decrease. After R_o > 1.3%, S_1 decreases rapidly and approaches zero.
2. T_{max}, (2+3) methylphenanthrene/(1+9) methylphenanthrene ((2+3)MP/(1+9)MP), and saturated+arene increase with the increase in R_o, while V_{daf} and the hydrogen-to-carbon ratio (H/C) decrease with the increase in R_o. The monotony of these parameters remains unchanged with the increase in R_o.
3. The range of $\delta^{13}C$ is about −25.8 to −22.9‰. It reaches a minimum at R_o = 1.4% and then becomes heavier gradually.
4. When R_o is greater than 1.3%, saturated/arene begins to decrease, and when R_o is greater than 1.7%, it basically ranges from 0.1 to 0.2.
5. Odd−even predominance (OEP), phytane/*n*-octadecane (Ph/nC_{18}), the normal alkane ratio ($\Sigma C_{21}^-/\Sigma C_{22}^+$), and 1460/1600, are abnormally elevated when R_o is between 1.6 and 2.0%. $\Sigma C_{21}^-/\Sigma C_{22}^+$ is the most obvious.
6. Pristane/phytane (Pr/Ph) suddenly decreases when R_o is greater than 1.7%.
7. Before R_o is greater than 1.8%, 1700/1600 decreases continuously and remains unchanged after R_o is greater than 1.8%.
8. 17α-22,29,30-Trinorhopane/18α-22,29,30-trinorhopane (Tm/Ts) decreases rapidly when R_o is greater than 0.7% and is extremely low when R_o is greater than 1.1%.

3.2. Hydrous Pyrolysis Characteristics. Hydrous pyrolysis of high-volatile bituminous coal[31] was conducted on Shanxi Formation gas coal in the Xiatuanbo Coal Mine, Huoxian, Qinshui Basin (Table 1).

Table 1. Vitrinite Reflectance and the Maceral Content of the Sample[a]

			maceral content (%)			
sample	R_o (%)	TOC (%)	*V*	*I*	*E*	*M*
XTB-1	0.86	62.61	46.0	10.5	31.3	11.8

[a]*V*, vitrinite; *I*, inertinite; *E*, exinite; *M*, mineral.

The gas generated in the experiment includes CH_4, H_2, CO_2, and C_{2-}. With the increase in experimental temperature, the gas yields of total gas, CH_4, H_2, and CO_2 all show an increasing trend. The variation trend of total gas and CH_4 gas yield is similar. The gas yield increases significantly after the simulated temperature is higher than 400 °C and reaches the first peak at about 450 °C and the second peak at about 550 °C. H_2 gas yield was significantly increased after 600 °C. The gas yield of CO_2 increases slowly with the increase in temperature, but the change is not obvious. However, C_{2-} is only produced before the temperature of 550 °C, and the yield is low, reaching the peak gas yield at about 450 °C (Figure 3a). However, the CH_4 yield at 600 °C obtained from the experiment was slightly lower than that of 550 °C, which may result from experimental error. Therefore, according to the increasing trend of CH_4 yield proposed by other reseachers[52,53] and the trend between 450 and 500 °C in our experiment, we revised the total gas and CH_4 yield at 600 °C. The R_o value obtained from the residue after the reaction is larger than the corresponding value in nature. Therefore, in order to facilitate the comparison with the

https://doi.org/10.1021/acsomega.1c02211
ACS Omega 2021, 6, 17660−17673

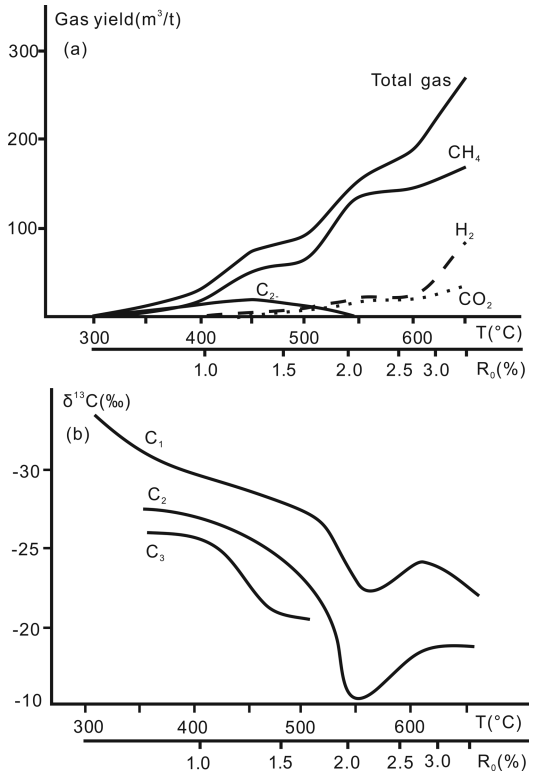

Figure 3. Gas generation characteristics in hydrous pyrolysis and isotopic characteristics: (a) gas generation characteristics (CH_4 yield at 600 °C was revised); (b) isotopic characteristics.

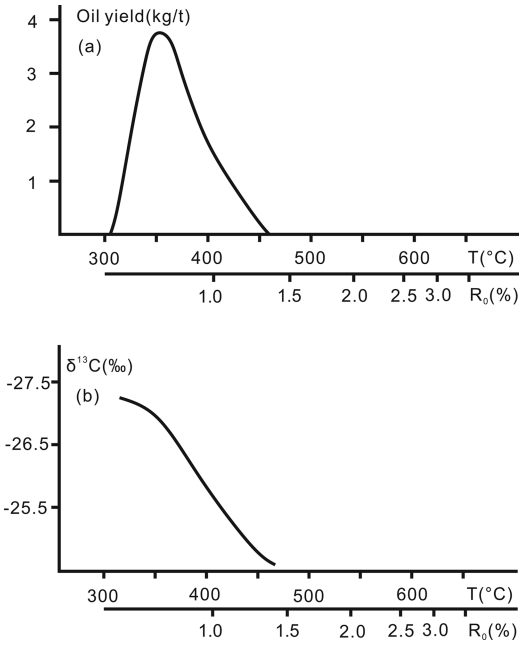

Figure 4. Oil generation characteristics in hydrous pyrolysis and isotopic characteristics: (a) oil generation characteristics; (b) isotopic characteristics.

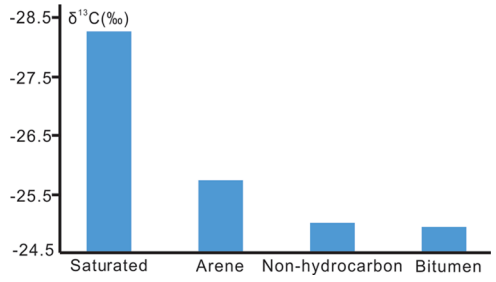

Figure 5. Carbon isotopic characteristics of oil components.

characteristics of natural thermal evolution, the corrected R_o was obtained according to the formula proposed by Zhang and Li.[54]

The result showed that $\delta^{13}C_1 < \delta^{13}C_2 < \delta^{13}C$, and a tendency of gradually becoming heavier as the temperature increased, but $\delta^{13}C_1$ and $\delta^{13}C_2$ suddenly became lighter and then heavier after the temperature is higher than 550 °C (Figure 3b).

In previous research,[52,53] the gas generation characteristics and the isotopic characteristics are similar to the results obtained in this paper. Methane production begins at 400 °C and slows down at 450−500 or 500−600 °C. C_{2-} mainly has significant output between 350 and 550 °C. H_2 and CO_2 will increase with the increase in temperature, and the rate of H_2 increases more obviously than that of CO_2.

Before the temperature of 500 °C, there was oil production (Figure 4a). At 350 °C, the yield was the highest and then gradually decreased.

The $\delta^{13}C$ of oil tends to become heavier as the temperature rises (Figure 4b). The $\delta^{13}C$ of different components are different, showing that $\delta^{13}C_{(\text{saturated hydrocarbon})} < \delta^{13}C_{(\text{arene})} < \delta^{13}C_{(\text{non-hydrocarbon})} < \delta^{13}C_{(\text{bitumen})}$ (Figure 5).

The organic geochemical analysis of soluble and insoluble organic matter collected from the reaction residue shows that its various characteristics with simulated temperature are similar to those of natural thermal evolution (Figure 6). The variation trend of S_1, HI, bitumen "A", H/C, $\delta^{13}C$, (2+3)MP/(1+9)MP, saturated/arene, saturated+arene, OEP, Pr/Ph, Ph/nC_{18}, $\Sigma C_{21}^{-}/\Sigma C_{22}^{+}$, 1400/1600, and 1400/760 is basically consistent with the natural thermal evolution. However, the variation trend of T_{max} and 1700/1600 is different from that of natural thermal evolution. T_{max} has a mutation at the simulated temperature of 400−450 °C. 1700/1600 gradually increased, and the trend was contrary to the natural thermal evolution.

4. DISCUSSION

4.1. Thermal Evolution Characteristics. *4.1.1. Thermal Evolution Stages and Characteristics.* According to natural thermal evolution (Figure 2), results of hydrous pyrolysis (Figures 3a, 4a, and 6), and references,[52,53] a more appropriate classification scheme of thermal evolution stages can be proposed, and the characteristics of each stage can be pointed out.

The thermal evolution stages of Late Paleozoic coal in the Qinshui Basin can be divided into the immature stage, symbiosis stage, wet gas stage, and dry gas stage, wherein the symbiosis stage can be divided into the preliminary stage and mainly gas stage (Table 2):

Immature Stage (R_o < 0.5%): All the parameters of organic geochemistry are relatively low, and some of them have an upward trend. This stage is when the most of kerogen has not yet begun cracking, and the hydrocarbon generation capacity of coal is extremely low.[52,55]

Preliminary Stage (0.5% < R_o < 0.7%): Some parameters such as S_1, S_1+S_2, HI, T_{max}, bitumen "A", total hydrocarbons, (2+3)MP/(1+9)MP, and saturated+arene keep rising. V_{daf}, H/C, and $\delta^{13}C$ have a declining trend. At this stage, the cracking rate of kerogen is accelerated, the yield of hydrocarbons is

https://doi.org/10.1021/acsomega.1c02211
ACS Omega 2021, 6, 17660−17673

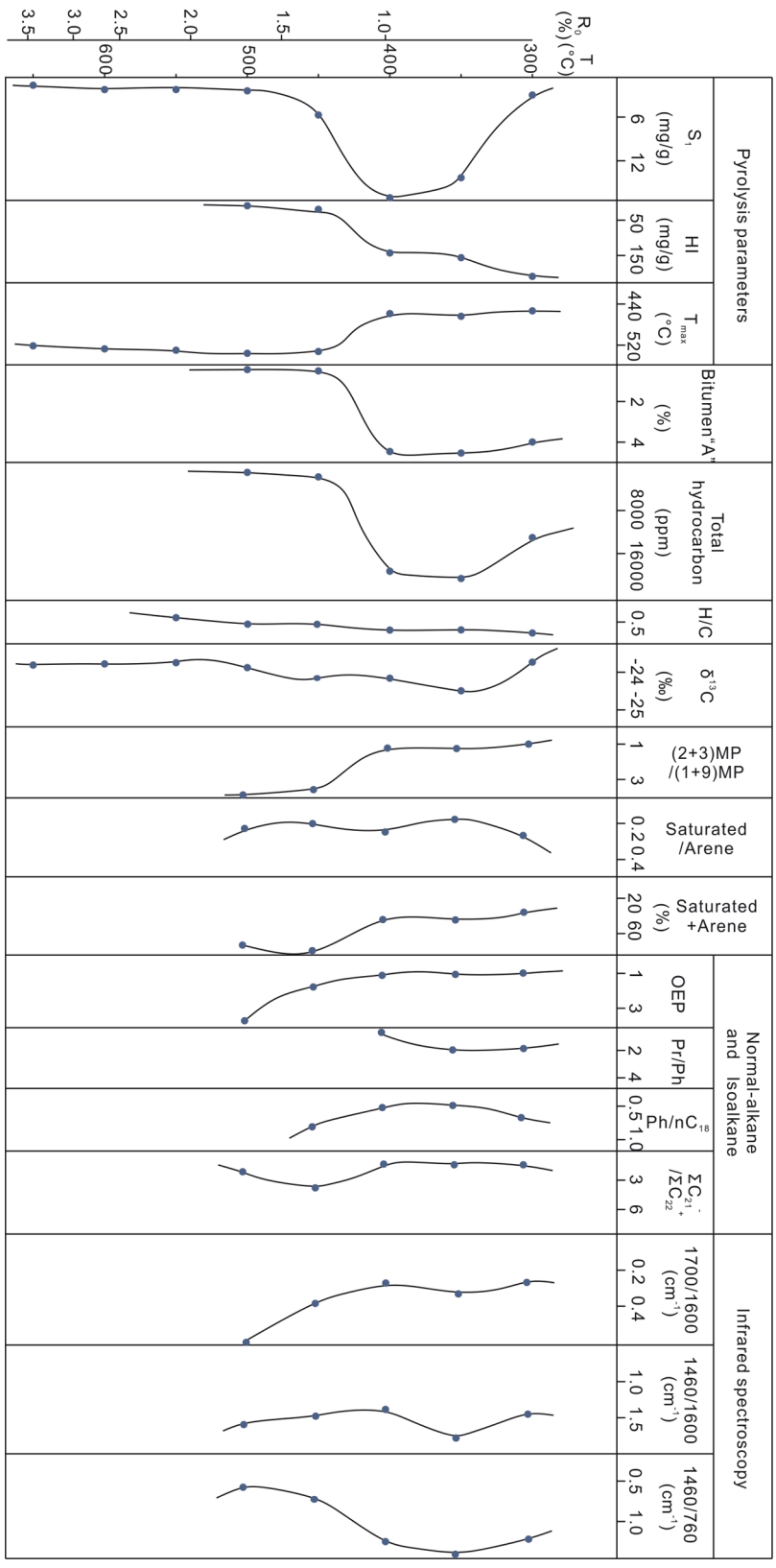

Figure 6. Geochemical characteristics of the soluble and insoluble organic matter from the reaction residue.

increased, and a small amount of oil and gas should be generated.[52,55]

Mainly Gas Stage ($0.7\% < R_o < 1.3\%$): S_1, S_1+S_2, HI, bitumen "A", and total hydrocarbons reached the peak and began to decline. 1700/1600 gradually decreases. Tm/Ts decreases rapidly and approaches 0. There is no change in the trend of T_{max}, (2+3)MP/(1+9)MP, saturated+arene, V_{daf}, and H/C. The $\delta^{13}C_1$, $\delta^{13}C_2$, $\delta^{13}C_3$, and $\delta^{13}C_{(oil)}$ all have a decreasing trend. The gaseous hydrocarbons, including CH_4 and C_{2-}, are generated with oil simultaneously. Also, the gaseous hydrocarbon yield

https://doi.org/10.1021/acsomega.1c02211
ACS Omega 2021, 6, 17660−17673

Table 2. Thermal Evolution Stages and Their Indexes of Organic Geochemical Parameters

stage	R_o (%)	T_{max} (°C)	(2+3)MP/(1+9)MP	saturated+arene (%)	V_{daf} (%)	H/C
immature	<0.5	<430	<1	<15	>40	>0.8
symbiosis						
preliminary	0.5−0.7	430−440	<1	15−20	35−40	0.78−0.8
mainly gas	0.7−1.3	440−467	1−1.7	20−25	25−35	0.64−0.78
wet gas	1.3−2.0	467−510	1.7−3.5	25−35	12−25	0.54−0.64
dry gas	>2.0	>510	>3.5	>35	<12	<0.54

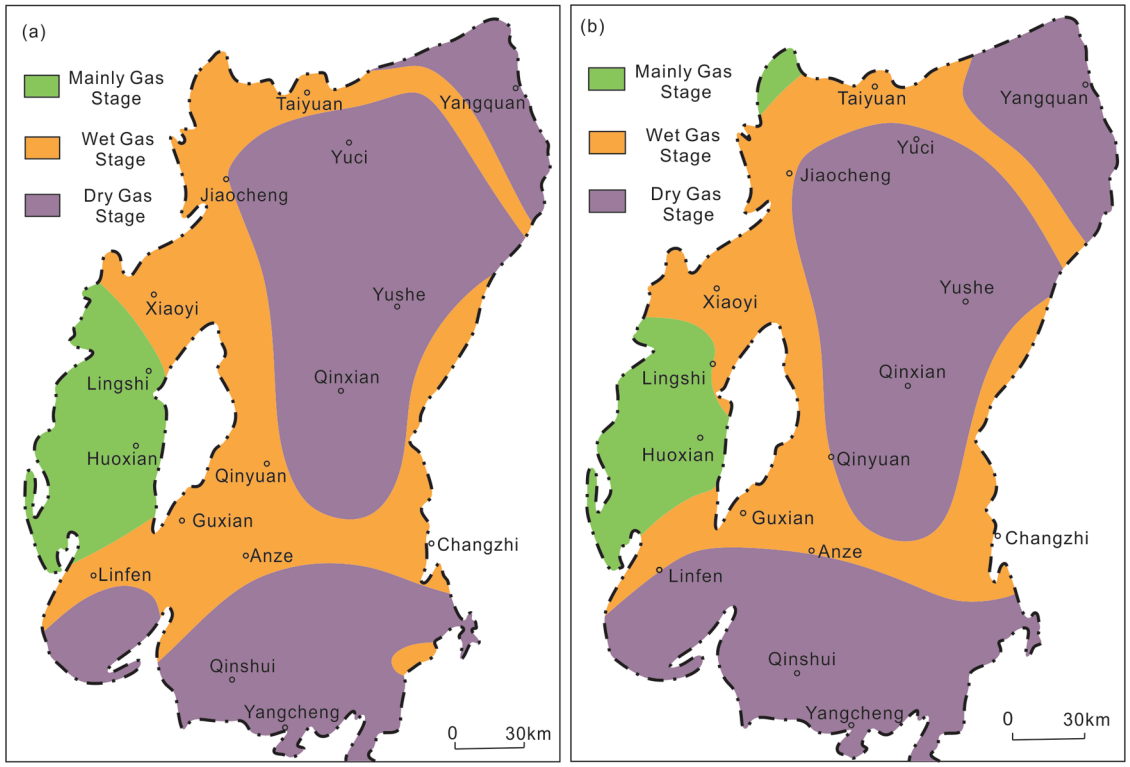

Figure 7. Plane distribution characteristics of thermal evolution stages in the Qinshui Basin: (a) Shanxi Formation; (b) Taiyuan Formation.

increases obviously, and the oil yield decreases. At this stage, the cracking rate of kerogen decreases. This stage is mainly heavier hydrocarbons cracking into the oil and gaseous hydrocarbons.

Wet Gas Stage ($1.3\% < R_o < 2.0\%$): S_1, S_1+S_2, HI, bitumen "A", and total hydrocarbons gradually decrease and approach 0. T_{max}, (2 + 3)MP/(1 + 9)MP, saturated+arene, V_{daf}, and H/C maintain the previous trend. $\delta^{13}C$ begins to increase, and saturated/arene begins to decrease. OEP, Ph/nC_{18}, $\Sigma C_{21}^-/\Sigma C_{22}^+$, and 1460/1600 are abnormally elevated. $\delta^{13}C_1$ and $\delta^{13}C_2$ become heavier faster. Almost no oil has been generated. The gaseous hydrocarbon yield increases rapidly, and the C_{2-} yield reaches the maximum. At this stage, kerogen cracking is basically completed. This stage is mainly oil and heavier gaseous hydrocarbons cracking into lighter gaseous hydrocarbons.

Dry Gas Stage ($R_o > 2.0\%$): Most of the parameters still maintain the trend of the last stage. The $\delta^{13}C_1$ would be lighter for a while then heavier again. The CH_4 yield increases continuously with the increase in temperature, and there is no oil and C_{2-} generation. At this stage, liquid hydrocarbon cracking is basically completed. This stage is mainly heavier gaseous hydrocarbons cracking into methane.

Except for R_o, some parameters such as T_{max}, (2+3)MP/(1+9)MP, saturated+arene, V_{daf}, and H/C remain monotonous with the increase of maturity, which can better indicate the boundary of the thermal evolution stage (Table 2).

4.1.2. Plane Distribution Characteristics of Thermal Evolution Stages. Based on the indexes of thermal evolution stages, the plane distribution characteristics of thermal evolution stages in the Qinshui Basin can be studied (Figure 7). The plane distribution characteristics of thermal evolution stages of the Shanxi Formation and Taiyuan Formation are very alike. Most of the areas have entered the dry gas stage. The dry gas stage is mainly distributed in the Yangquan area in the north of the basin, the Yuci-Qinyuan area in the middle of the basin, and the Linfen-Yangcheng area in the south. The Lingshi-Huoxian area in the west of the basin has a relatively low thermal evolution stage, which is the oil−gas stage of the symbiosis stage. The rest of the basin is basically in the wet gas stage.

4.2. Gas Generation Characteristics. *4.2.1. Gas Generation Rate.* The R_o of high-volatile bituminous coal used in hydrous pyrolysis is 0.86%. Therefore, according to the results of hydrous pyrolysis, refer to the previous studies,[52−54,56,57] the gas generation rate (Figure 8) at different R_o of the Late Paleozoic coal in the Qinshui Basin was sorted out. The gas generation rate can be used to calculate the gas generation strength and further calculate the number of resources. It can be found that coal begins to produce gas relatively early, but when the meta-

https://doi.org/10.1021/acsomega.1c02211
ACS Omega 2021, 6, 17660−17673

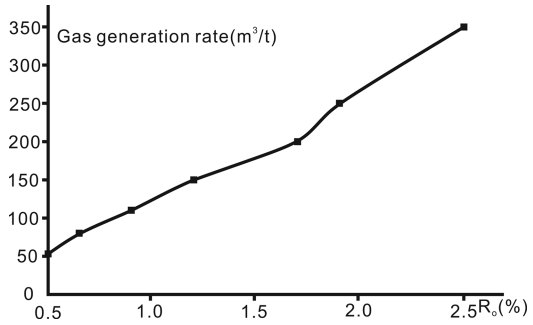

Figure 8. Gas generation rates at different R_o.

morphism degree of coal is equal to or lower than that of fat coal (R_o < 1.2%), the gas generation rate is low and increases slowly, and then, the gas generation rate increases rapidly. When the coal rank reaches anthracite (R_o > 2.5%), the gas generation rate of Late Paleozoic coal has reached 350 m^3/t.

4.2.2. Plane Distribution Characteristics of Gas Generating Strength. Using the formula $Q_c = M_c S_c D_c g_c \times 10^{-2}$, the gas generating strength of the Late Paleozoic coal in the Qinshui Basin was calculated.

Q_c is the gas generating strength of coal (10^8 m^3/km).
M_c is the thickness of coal (m).
S_c is the area of coal (km^3).
D_c is the specific gravity of coal (t/m^3).
g_c is the gas generation rate of coal (m^3/t).

The thickness and R_o of coal involved in the calculation are mainly from the measured value, and some of them are inferred by referring to the previous study[58] and the isopachs of coals and the contour map of R_o (Figure 9). The specific gravity of bituminous coal is 1.4 t/m^3, and that of anthracite is 1.6 t/m^3.

The contour map shows that the gas generating strength of the Taiyuan Formation is higher than that in the Shanxi Formation (Figure 10). Also, the characteristics of the two Formation are different. In the Shanxi Formation, the Yangcheng area in the southern part of the basin has the highest gas generating strength, which basically exceeds 50 × 10^8 m^3/km^2. Meanwhile, in the Taiyuan Formation, the northern part of the basin has a relatively high gas generating strength, and the Yangquan area is the gas generation center of the Taiyuan Formation, whose gas generating strength basically exceeds 80 × 10^8 m^3/km^2.

4.3. Thermal Evolution and the Free Gas Accumulation Model. The studies show that the cumulative quantity of gas generated from coal is 6−10 times larger than its saturated adsorption capacity,[27,59,60] so much gas can migrate out of the coal seam and be accumulated in other strata in the basin to form the coal measure free gas reservoirs,[26,27,46,59] and the coal measure free gas reservoirs are more similar to conventional natural gas reservoirs, which have higher requirements for the gas generation, reservoir, cap rock, trap, migration, and preservation, as well as their spatio-temporal configuration relations.

According to the geothermal gradient,[26] the measured R_o values, local tectonic events,[61] thermal evolution stages, gas generation rates at different R_o (Figure 8), and other data,[27,30,60] thermal evolution and the free gas accumulation model can be pointed out (Figure 11).

The model shows that the highest temperature of the source rocks in the Shanxi Formation and the Taiyuan Formation can reach 240 °C. Source rocks first experienced initial burial and warming after deposition. In the Early Triassic, the thermal evolution stage entered the preliminary stage of the symbiosis stage, and in the Late Triassic, the thermal evolution stage entered the mainly gas stage. Subsequently, due to the small-scale uplift and erosion, the temperature fluctuated, and the thermal evolution was slow from the Late Triassic to the Middle-Late Jurassic. In the Middle-Late Jurassic, the temperature increased rapidly to the maximum value, and the thermal evolution stage entered the wet gas stage and then quickly entered and stayed at the dry gas stage in the Late Jurassic.

The main source rock, reservoir, and cap rock of free gas began to form in the Late Carboniferous, and the source rock and reservoir were basically formed in the Middle-Late Permian, while the formation time of the cap rock lasted until the end of Permian. From the Middle Triassic to the Late Triassic, the first gas generation occurred, but the formation of the traps in the basin began in the Jurassic and lasted until the Neogene-Quaternary under the influence of tectonism. The second gas generation period lasted from the Late Jurassic to the Early Cretaceous. From the beginning of the first gas generation period, the Middle Triassic, the migration and accumulation of gases began. Also, under the influence of tectonism, the gas reservoir was continuously altered, and gas migration and accumulation continued until the Neogene-Quaternary.

Therefore, the spatio-temporal configuration relation of the first gas generation stage is very poor, and the trap in the basin has not been formed during the gas generation and migration, so it is difficult to form the free gas reservoir. The second gas generation stage is more important because it not only generated a large amount of gas but also had a good spatio-temporal configuration relation, which is conducive to the formation of a large number of free gas reservoirs.

4.4. Contrast with the Ordos Basin. The Ordos Basin, located on the west side of the Qinshui Basin, is one of the hot research areas in recent years. Many gas reservoirs with Paleozoic coal-bearing strata as source rocks have been found.[11,62] The two basins are similar in terms of tectonic evolution and the sedimentary environment.[39,63] Therefore, the comparison of hydrocarbon generation and accumulation characteristics of source rocks between the two basins is conducive to in-depth study and long-term evaluation of coalbed methane resources in the Qinshui Basin.

The Late Paleozoic coal seams are the important hydrocarbon source rocks of the two basins.[64] The gas generation capacity of the coal from the Shanxi Formation in the Ordos Basin is stronger, and the oil generation capacity is much stronger (Table 3). Previous research shows that the CH_4 yield can reach 153.68 $mg/g_{(TOC)}$ (equal to 234.63 $mL/g_{(TOC)}$ because $\rho_{(CH4)}$ = 0.655 g/L at 101.325 kPa and 25 °C) and 139.09 $mL/g_{(coal)}$, and the oil yield can reach 171.65 $mg/g_{(TOC)}$[62] (Table 3). However, in the Qinshui Basin, the CH_4 yield can only reach 171.69 $mL/g_{(TOC)}$ and 129.81 $mL/g_{(coal)}$, and the oil yield can only reach 45.94 $mg/g_{(coal)}$[53] (Table 3).

Different from the Qinshui Basin, the Ordos Basin may have a weaker tectonic influence. Under such a condition, there may be only one gas generation stage of the coal and coal measure mudstone or shale (because of the same tectonic activities and formation, the coal may have much similar gas generation stages to the coal measure mudstone or shale) from the Shanxi and the Taiyuan Formation[66,67] (Figure 12a), or the interval between two gas generation stages is much shorter and the generation times are longer than that in the Qinshui Basin[68,69] (Figure 12b). According to Figure 12a, the gas generation stage lasted for

https://doi.org/10.1021/acsomega.1c02211
ACS Omega 2021, 6, 17660−17673

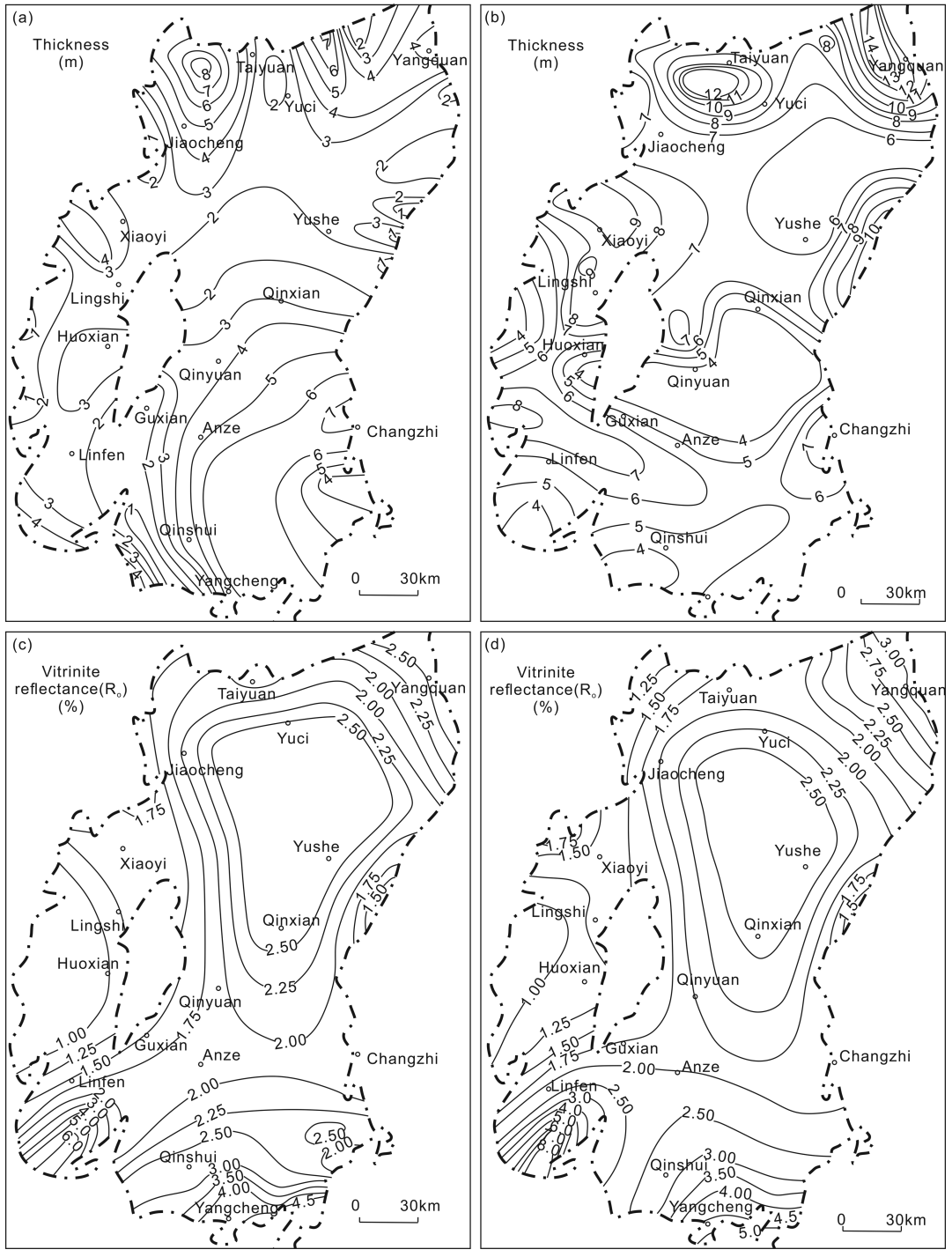

Figure 9. Isopachs of coals and the contours of R_o of the Taiyuan and the Shanxi Formations of the Qinshui Basin: (a) isopachs of coals of the Shanxi Formation; (b) isopachs of coals of the Taiyuan Formation; (c) contours of R_o of the Shanxi Formation; (d) contours of R_o of the Taiyuan Formation.

about 150 Ma. According to Figure 12b, the first gas generation stage lasted for about 40 Ma, the second gas generation stage lasted for about 30 Ma, and the interval lasted for about only 15 Ma. However, in the Qinshui Basin, according to Figure 11, the first gas generation stage lasted for about only 20 Ma, the second gas generation stage lasted for about only 30 Ma, and the interval lasted for about 65 Ma.

Therefore, the coal in the Ordos Basin has better hydrocarbon generation capacity and longer and more continuous gas generation time than the Qinshui Basin. This indicates that the Ordos Basin may have better prospects for exploration and development.

5. CONCLUSIONS

The characteristics of natural thermal evolution show that the variation trends of various geochemical parameters are different with the increase in R_o. Hydrous pyrolysis shows that the gas production potential of coal is excellent, but the oil production potential is poor. The gases produced consist mainly of CH_4, C_{2-}, CO_2, and H_2. C_{2-} is produced only before the simulated temperature of 550 °C, and oil is produced only before the

https://doi.org/10.1021/acsomega.1c02211
ACS Omega 2021, 6, 17660−17673

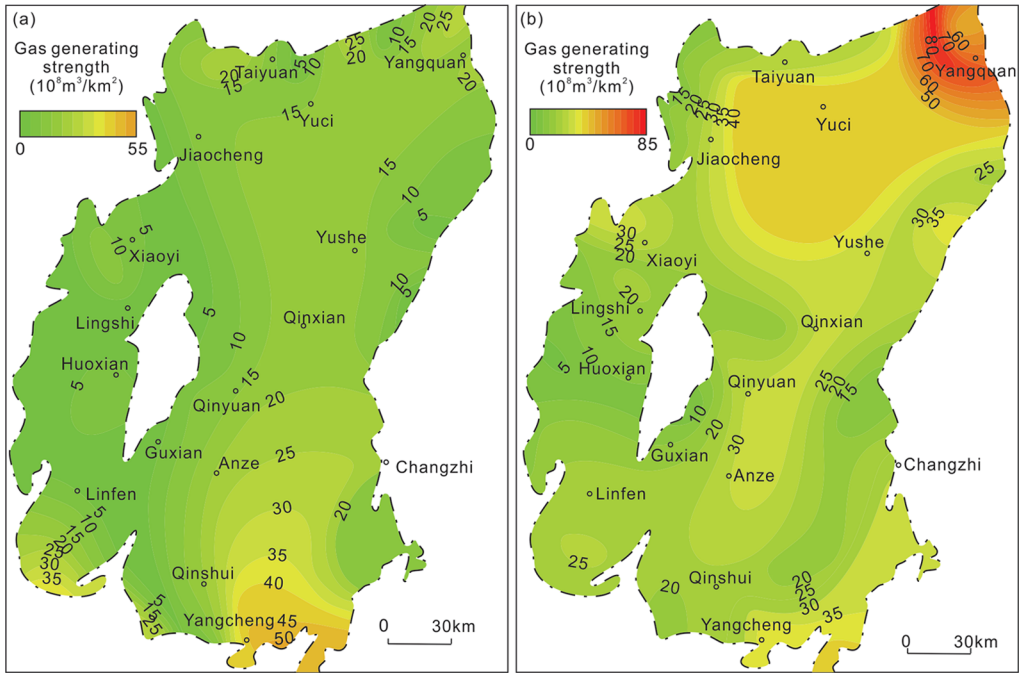

Figure 10. Gas generation strength contour map of the Late Paleozoic coal in the Qinshui Basin: (a) Shanxi Formation; (b) Taiyuan Formation.

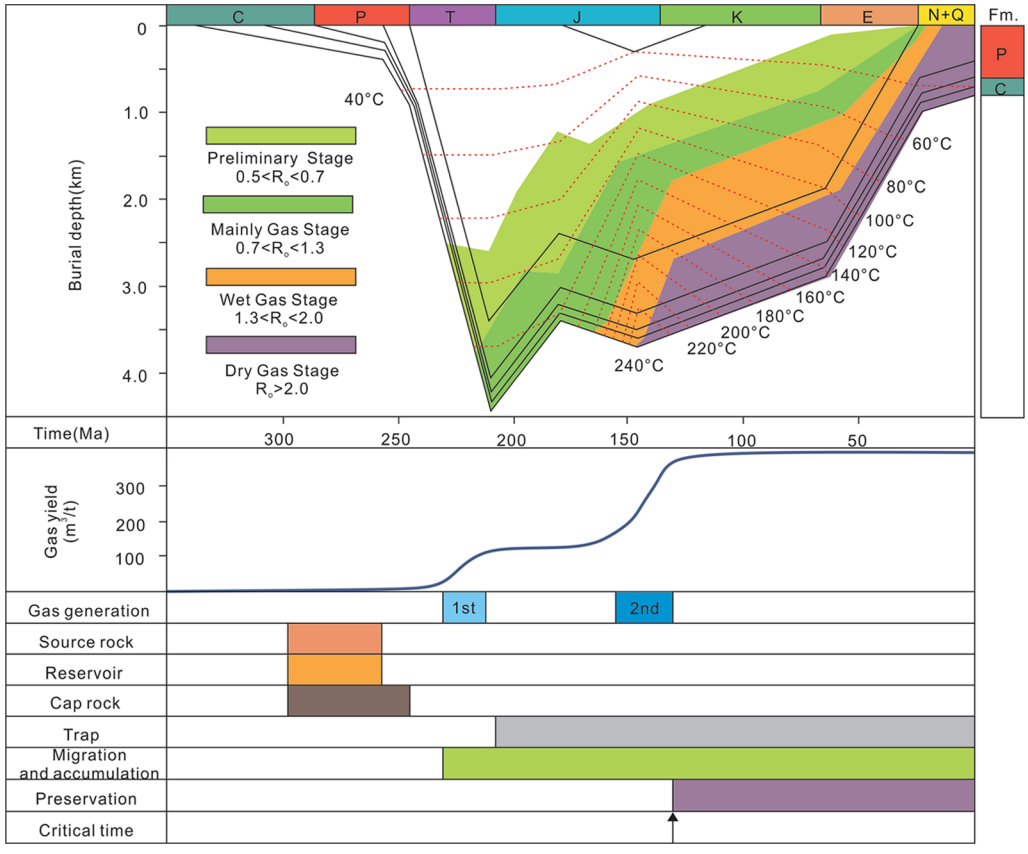

Figure 11. Thermal evolution and the free gas accumulation model of the Qinshui Basin (modified from refs 27 and 30). Reprinted (Adapted or Reprinted in part) with permission from ref 27. Copyright 2018 Elsevier. Reprinted (Adapted or Reprinted in part) with permission from ref 30. Copyright 2005 AAPG.

temperature of 500 °C. The result shows that $\delta^{13}C_1 < \delta^{13}C_2 < \delta^{13}C_3$, and $\delta^{13}C$ becomes heavier with the increase in temperature, but $\delta^{13}C_1$ and $\delta^{13}C_2$ would be lighter after the temperature of 550 °C then heavier again. The $\delta^{13}C$ of oil becomes heavier as the temperature increases, and the result shows that $\delta^{13}C_{(\text{saturated hydrocarbon})} < \delta^{13}C_{(\text{arene})} < \delta^{13}C_{(\text{non-hydrocarbon})} < \delta^{13}C_{(\text{bitumen})}$.

https://doi.org/10.1021/acsomega.1c02211
ACS Omega 2021, 6, 17660−17673

Table 3. Hydrocarbon Generation Capacity of the Upper Paleozoic Coal in the Ordos Basin and the Qinshui Basin[52,53,62,65]

basin	area	formation	CH_4	C_{2-}	oil
Ordos[62]	Shenfu	Shanxi	153.68 (mg/$g_{(TOC)}$; 20 °C/h; 600 °C)	36.18 (mg/$g_{(TOC)}$; 20 °C/h; 482 °C)	171.65 (mg/$g_{(TOC)}$; 20 °C/h; 417 °C)
Ordos[65]	Eastern edge		139.09 (mL/$g_{(coal)}$; 20 °C/h; 610 °C)	10.90 (mL/$g_{(coal)}$; 20 °C/h; 455 °C)	
Qinshui[52]	Liyazhuang	Shanxi	171.69 (mL/$g_{(TOC)}$; 20 °C/h; 600 °C)	17.83 (mL/$g_{(TOC)}$; 20 °C/h; 490 °C)	
Qinshui[53]	Huoxian	Shanxi	95.11 (mL/$g_{(coal)}$; 600 °C)	35.56 (mL/$g_{(coal)}$; 400 °C)	45.94 (mg/$g_{(coal)}$; 350 °C)
			130.30 (mL/$g_{(coal)}$; 650 °C)		
Qinshui	Xiatuanbo	Shanxi	129.81 (mL/$g_{(coal)}$; 600 °C)	18.78 (mL/$g_{(coal)}$; 450 °C)	3.77 (mg/$g_{(coal)}$; 350 °C)
			169.23 (mL/$g_{(coal)}$; 650 °C)		

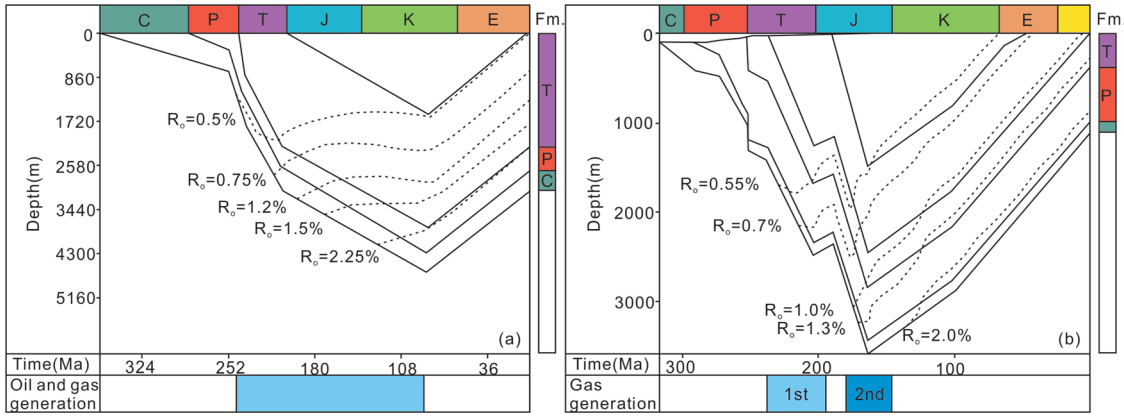

Figure 12. Gas generation and accumulation patterns of the Ordos Basin: (a) only one oil and gas generation stage (modified from ref 67); (b) two stages but the time is longer and the interval is shorter (modified from ref 69). Reprinted (Adapted or Reprinted in part) with permission from ref 67. Copyright 2005 Elsevier. Reprinted (Adapted or Reprinted in part) with permission from ref 69. Copyright 2020 Elsevier.

The thermal evolution stages can be divided into four stages: the immature stage, symbiosis stage, wet gas stage, and dry gas stage, wherein the symbiosis stage can be divided into the preliminary stage and mainly gas stage. T_{max}, (2+3)MP/(1+9)MP, saturated+arene, V_{daf}, and H/C can better indicate the boundary of the thermal evolution stage. In the plane, the northern, central, and southern parts of the basin are mainly in the dry gas stage, the western part is in the mainly gas stage, and the other parts are in the wet gas stage.

The gas generating strength of the Taiyuan Formation is higher than that in the Shanxi Formation. Also, the gas generation center of the Shanxi Formation is the Yangcheng area in the southern part of the basin. Meanwhile, in the Taiyuan Formation, the gas generation center is the Yangquan area in the northern part of the basin.

There are two gas generation periods in the Qinshui basin. The first period started at the Late Triassic, basically corresponding to the mainly gas stage. The second period started at the Middle-Late Jurassic, basically corresponding to the wet gas and dry gas stage. Also, the gas production in the second period is larger, and the spatio-temporal configuration relationship is better.

Compared with the Ordos Basin, the hydrocarbon generation capacity of the Late Paleozoic coal in the Qinshui Basin is relatively poor, especially the oil generation capacity, and the gas generation time of coal and coal measure mudstone or shale in the Ordos Basin is longer and more continuous. Therefore, the exploration and development prospect of the Ordos Basin is better.

6. METHODS

6.1. Organic Geochemistry Analysis. Under the guidance of the Chinese Oil and Gas Industry Standard and the protocols of the International Committee for Coal and Organic Petrology (ICCP), R_o was measured using an AXIO Imager Mlm microphotometer.[70] Also, to minimize error, 100 points were measured for each sample. Dry-ash-free volatiles (V_{daf}) were determined by conventional industrial analysis.

Using a Leco CS-230 analyzer to measure the total organic carbon (TOC) content, about 100 mg of coal samples was selected and crushed into particles with a diameter of less than 0.2 mm. Inorganic carbon was removed by adding boiling hydrochloric acid, and then, hydrochloric acid was drained. Next, the sample residue was burned, and the TOC content was calculated.[71]

We cut off a cube with a side length of 2 cm from each sample and treated it with two-component epoxy resin. The treated sample is polished and then viewed under a Zeiss Axioplan microscope 500 times larger. The maceral groups were divided into vitrinite, inertinite, exinite, and mineral by making 500 counts on every treated sample.[48] Elements (C, H, N, and S) were determined using a Carlo Erba EA 1108 apparatus and using sulfanilamide as a standard.[72] Organic matter (saturated hydrocarbon, arene hydrocarbon, non-hydrocarbon, and bitumen) extraction was carried out by conventional organic geochemical methods. Components were extracted by conventional organic geochemistry.

Stable carbon isotope ($\delta^{13}C$) analysis was performed using an MAT271 spectrometer. Also, the analysis was carried out under the condition where the electron energy is 68 eV, the mass resolution rate is 200, the vacuum degree is less than 2×10^{-6} Pa, and the emission current is 0.800 mA.

Parameters such as the soluble hydrocarbon content (S_1), pyrolysis hydrocarbon content (S_2), hydrogen index (HI), and maximum pyrolysis temperature (T_{max}) were analyzed using a ROCK-EVAL6 rock pyrolysis analyzer. S_1 needs to be measured

https://doi.org/10.1021/acsomega.1c02211
ACS Omega 2021, 6, 17660−17673

at an oven temperature of 300 °C, while S_2 needs to rise to 550 °C at a rate of 25 °C per minute.[73,74]

Using an Agilent 7890 gas chromatograph with 5975C mass spectrometers to analyze the molecular composition, the temperature for analysis was 60 °C first. After 2 min, the temperature increased to 300 °C with a speed of 2 °C/min and kept at 300 °C for 30 min.[70] Samples were determined using a Vertex 70 infrared spectrometer. First, the coal sample was mixed with 100 mg of potassium bromide in the ratio of 1:100 then ground and then put into the mold. Using a tablet press, we applied vacuum pressure to 90,000 N·cm^{-2} for 1 min, and then, an infrared spectrometer was used to scan the measurement background, and then, the pressed sheet was put into the infrared spectrometer for testing, a total of 16 times of scanning.

6.2. Hydrous Pyrolysis. The experimental samples of hydrous pyrolysis were crushed into fragments of about 1 mm and screened to remove fine particles and ensure their complete homogeneity. About 10 g of samples was added to 15 mL of distilled water, and the coal particles were soaked in water. Before heating, we checked whether there was air leakage in the container and rinsed air inside the container with helium at a pressure of 5 MPa and finally kept the air pressure inside the container at about 5 MPa. Then, the samples were heated for a short time and kept at a constant temperature for 24 h. The lowest simulated temperature was 300 °C, and every 50 °C is an experimental point, a total of eight experimental points. After cooling to room temperature, gaseous hydrocarbons were collected with water displacement. The liquid hydrocarbon discharged also includes the part adsorbed on the sample surface and the container wall, which is cleaned with dichloromethane and filtered with filter paper at least three times. The compositions and carbon isotopes of the collected gaseous and liquid hydrocarbons were analyzed. After the reaction, the soluble and insoluble organic matter collected from the reaction residue was analyzed the same as coal samples.[75−77]

AUTHOR INFORMATION

Corresponding Author

Wenhui Huang − *School of Energy Resources, China University of Geosciences (Beijing), Beijing 100083, China;* orcid.org/0000-0002-9623-2652; Email: huangwh@cugb.edu.cn

Authors

Ruilin Hao − *School of Energy Resources, China University of Geosciences (Beijing), Beijing 100083, China*

Bo Jiu − *School of Energy Resources, China University of Geosciences (Beijing), Beijing 100083, China*

Complete contact information is available at: https://pubs.acs.org/10.1021/acsomega.1c02211

Author Contributions

R.H. wrote the original draft; W.H. contributed to resources and review and editing of the manuscript and performed supervision; B.J. contributed to the review and editing of the manuscript.

Notes

The authors declare no competing financial interest.

ACKNOWLEDGMENTS

This work received financial support from the "National Natural Science Foundation of China" (grant nos. 41972172 and U1910205).

REFERENCES

(1) Hill, R. J.; Zhang, E.; Katz, B. J.; Tang, Y. Modeling of gas generation from the Barnett Shale, Fort Worth Basin, Texas. *AAPG Bull.* **2007**, *91*, 501−521.

(2) Green, M. S.; Flanegan, K. C.; Gilcrease, P. C. Characterization of a methanogenic consortium enriched from a coalbed methane well in the Powder River Basin, U.S.A. *Int. J. Coal Geol.* **2008**, *76*, 34−45.

(3) Guo, H.; Zhang, Y.; Zhang, J.; Huang, Z.; Urynowicz, M. A.; Liang, W.; Han, Z.; Liu, J. Characterization of anthracite-degrading methanogenic microflora enriched from Qinshui Basin in China. *Energy Fuels* **2019**, *33*, 6380−6389.

(4) Gentzis, T. Stability analysis of a horizontal coalbed methane well in the Rocky Mountain Front Ranges of southeast British Columbia, Canada. *Int. J. Coal Geol.* **2009**, *77*, 328−337.

(5) Gentzis, T.; Goodarzi, F.; Cheung, F. K.; Laggoun-Défarge, F. Coalbed methane producibility from the Mannville coals in Alberta, Canada: A comparison of two areas. *Int. J. Coal Geol.* **2008**, *74*, 237−249.

(6) McGlade, C.; Speirs, J.; Sorrell, S. Unconventional gas − A review of regional and global resource estimates. *Energy* **2013**, *55*, 571−584.

(7) Zou, C.; Zhai, G.; Zhang, G.; Wang, H.; Zhang, G.; Li, J.; Wang, Z.; Wen, Z.; Ma, F.; Liang, Y.; et al. Formation, distribution, potential and prediction of global conventional and unconventional hydrocarbon resources. *Pet. Explor. Dev.* **2015**, *42*, 14−28.

(8) Shi, J.; Zeng, L.; Dong, S.; Wang, J.; Zhang, Y. Identification of coal structures using geophysical logging data in Qinshui Basin, China: Investigation by kernel Fisher discriminant analysis. *Int. J. Coal Geol.* **2020**, *217*, 103314.

(9) Shi, J.; Zeng, L.; Zhao, X.; Zhang, Y.; Wang, J. Characteristics of natural fractures in the upper Paleozoic coal bearing strata in the southern Qinshui Basin, China: Implications for coalbed methane (CBM) development. *Mar. Pet. Geol.* **2020**, *113*, 104152.

(10) Feng, Q.; Kang, Y.; Huang, F. Experimental evaluation of permeability damage to No.15 coal seam in the Qinshui Basin. *Acta Geol. Sin. (Engl. Ed.)* **2015**, *89*, 383−385.

(11) Liu, Y.; Xu, H.; Tang, D.; Xu, F.; Mathews, J. P.; Hou, W.; Yan, X.; Ding, F. Coalbed methane production of a heterogeneous reservoir in the Ordos Basin, China. *J. Nat. Gas Sci. Eng.* **2020**, *82*, 103502.

(12) Zhang, J.; Feng, Q.; Zhang, X.; Hu, Q.; Wen, S.; Chen, D.; Zhai, Y.; Yan, X. Multi-fractured horizontal well for improved coalbed methane production in eastern Ordos basin, China: Field observations and numerical simulations. *J. Pet. Sci. Eng.* **2020**, 107488.

(13) Zou, C.; Yang, Z.; Sun, S.; Zhao, Q.; Bai, W.; Liu, H.; Pan, S.; Wu, S.; Yuan, Y. "Exploring petroleum inside source kitchen:" Shale oil and gas in Sichuan Basin. *Sci. China Earth Sci.* **2020**, *63*, 934−953.

(14) Zou, C.; Yang, Z.; Dai, J.; Dong, D.; Zhang, B.; Wang, Y.; Deng, S.; Huang, J.; Liu, K.; Yang, C.; Wei, G.; Pan, S. The characteristics and significance of conventional and unconventional Sinian−Silurian gas systems in the Sichuan Basin, central China. *Mar. Pet. Geol.* **2015**, *64*, 386−402.

(15) Lau, H. C.; Li, H.; Huang, S. Challenges and opportunities of coalbed methane development in China. *Energy Fuels* **2017**, *31*, 4588−4602.

(16) Li, M.; Jiang, B.; Miao, Q.; Wang, G.; You, Z.; Lan, F. Multi-Phase tectonic movements and their controls on coalbed methane: A case study of No. 9 coal seam from Eastern Yunnan, SW China. *Energies* **2020**, *13*, 6003.

(17) Wang, Y.; Liu, D.; Cai, Y.; Li, X. Variation of petrophysical properties and adsorption capacity in different rank coals: An experimental study of coals from the Junggar, Ordos and Qinshui Basins in China. *Energies* **2019**, *12*, 986.

(18) Zhang, J.; Liu, D.; Cai, Y.; Pan, Z.; Yao, Y.; Wang, Y. Geological and hydrological controls on the accumulation of coalbed methane within the No. 3 coal seam of the southern Qinshui Basin. *Int. J. Coal Geol.* **2017**, *182*, 94−111.

(19) Wang, F.; Yin, S. Hydrocarbon generation potential of the C-P continental source rocks in the Qinshui Basin. *Pet. Sci. Technol.* **2019**, *37*, 208−214.

(20) Zou, C.; Zhang, G.; Tao, S.; Hu, S.; Li, X.; Li, J.; Dong, D.; Zhu, R.; Yuan, X.; Hou, L.; et al. Geological features, major discoveries and unconventional petroleum geology in the global petroleum exploration. *Pet. Explor. Dev.* **2010**, *37*, 129−145.
(21) Gottardi, R.; Adams, L. M.; Borrok, D.; Teixeira, B. Hydrocarbon source rock characterization, burial history, and thermal maturity of the Steele, Niobrara and Mowry Formations at Teapot Dome, Wyoming. *Mar. Pet. Geol.* **2019**, *100*, 326−340.
(22) Zhu, H.; Ju, Y.; Huang, C.; Chen, F.; Chen, B.; Yu, K. Microcosmic gas adsorption mechanism on clay-organic nanocomposites in a marine shale. *Energy* **2020**, 117256.
(23) Lv, Y.; Tang, D.; Xu, H.; Luo, H. Production characteristics and the key factors in high-rank coalbed methane fields: A case study on the Fanzhuang Block, Southern Qinshui Basin, China. *Int. J. Coal Geol.* **2012**, *96-97*, 93−108.
(24) Meng, Z.; Zhang, J.; Wang, R. In-situ stress, pore pressure and stress-dependent permeability in the Southern Qinshui Basin. *Int. J. Rock Mech. Min. Sci.* **2011**, *48*, 122−131.
(25) Su, X.; Lin, X.; Liu, S.; Zhao, M.; Song, Y. Geology of coalbed methane reservoirs in the Southeast Qinshui Basin of China. *Int. J. Coal Geol.* **2005**, *62*, 197−210.
(26) Yu, K.; Ju, Y.; Zhang, B. Modeling of tectono-thermal evolution of Permo-Carboniferous source rocks in the southern Qinshui Basin, China: Consequences for hydrocarbon generation. *J. Pet. Sci. Eng.* **2020**, *193*, 107343.
(27) Li, J.; Tang, S.; Zhang, S.; Li, L.; Wei, J.; Xi, Z.; Sun, K. Characterization of unconventional reservoirs and continuous accumulations of natural gas in the Carboniferous-Permian strata, mid-eastern Qinshui basin, China. *J. Nat. Gas Sci. Eng.* **2018**, *49*, 298−316.
(28) Dieckmann, V.; Schenk, H. J.; Horsfield, B.; Welte, D. H. Kinetics of petroleum generation and cracking by programmed-temperature closed-system pyrolysis of Toarcian Shales. *Fuel* **1998**, *1/2*, 23−31.
(29) Duan, Y.; Wu, B.; Zheng, C.; Wang, C.; Zhang, H.; Tao, M.; Liu, J.; Zhang, J. Kinetics of coal hydrocarbon generation in Qinshui basin, Shanxi. *Chin. Sci. Bull.* **2005**, *50*, 1405−1411.
(30) Su, X.; Lin, X.; Zhao, M.; Song, Y.; Liu, S. The upper Paleozoic coalbed methane system in the Qinshui basin, China. *AAPG Bull.* **2005**, *89*, 81−100.
(31) In *ASTM Standard D388-19a*; ASTM International: West Conshohocken, PA, 2019.
(32) Luo, X.; Gong, S.; Sun, F. J.; Wang, Z. H.; Qi, J. S. Effect of volcanic activity on hydrocarbon generation: Examples in Songliao, Qinshui, and Bohai Bay Basins in China. *J. Nat. Gas Sci. Eng.* **2017**, *38*, 218−234.
(33) Zhang, J.; Feng, Q.; Zhang, X.; Hu, Q.; Yang, J.; Wang, N. A novel data-driven method to estimate methane adsorption isotherm on coals using the gradient boosting decision tree: A case study in the Qinshui Basin, China. *Energies* **2020**, *13*, 5369.
(34) Zou, Z.; Liu, D.; Cai, Y.; Wang, Y.; Li, J. Geological factors and reservoir properties affecting the gas content of coal seams in the Gujiao Area, Northwest Qinshui Basin, China. *Energies* **2018**, *11*, 1044.
(35) Liu, D.; Wang, Y.; Ni, X.; Tao, C.; Fan, J.; Wu, X.; Zhao, S. Classification of coal structure combinations and their influence on hydraulic fracturing: A case study from the Qinshui Basin, China. *Energies* **2020**, *13*, 4559.
(36) Qiu, N.; Zuo, Y.; Chang, J.; Li, W. Geothermal evidence of Meso-Cenozoic lithosphere thinning in the Jiyang sub-basin, Bohai Bay Basin, eastern North China Craton. *Gondwana Res.* **2014**, *26*, 1079−1092.
(37) Zhu, R.; Chen, L.; Wu, F.; Liu, J. Timing, scale and mechanism of the destruction of the North China Craton. *Sci. China Earth Sci.* **2011**, *54*, 789−797.
(38) Zhang, H.; Liu, D.; Yao, Y.; Xie, S.; Liu, J.; Li, Z. The control of structure on coalbed methane (CBM) enrichment in Zhengzhuang Block of Qinshui Basin, China. *Appl. Mech. Mater.* **2013**, *295-298*, 3346−3349.
(39) Ritts, B. D.; Hanson, A. D.; Darby, B. J.; Nanson, L.; Berry, A. Sedimentary record of Triassic intraplate extension in North China: evidence from the nonmarine NW Ordos Basin, Helan Shan and Zhuozi Shan. *Tectonophysics* **2004**, *386*, 177−202.
(40) Sun, B. L.; Zeng, F. G.; Xia, P.; Zhu, Y. R.; Liu, C. Late Triassic-Early Jurassic abnormal thermal event constrained by zircon fission track dating and vitrinite reflectance in Xishan coalfield, Qinshui Basin, central North China. *Geol. J.* **2018**, *53*, 1039−1049.
(41) Kusky, T. M.; Polat, A.; Windley, B. F.; Burke, K. C.; Dewey, J. F.; Kidd, W. S. F.; Maruyama, S.; Wang, J.; Deng, H.; Wang, Z.; Wang, C.; Fu, D.; Li, X. W.; Peng, H. T. Insights into the tectonic evolution of the North China Craton through comparative tectonic analysis: A record of outward growth of Precambrian continents. *Earth-Sci. Rev.* **2016**, *162*, 387−432.
(42) Shao, L.; Yang, Z.; Shang, X.; Xiao, Z.; Wang, S.; Zhang, W.; Zheng, M.; Lu, J. Lithofacies palaeogeography of the Carboniferous and Permian in the Qinshui Basin, Shanxi Province, China. *J. Palaeogeogr.* **2015**, *4*, 387−413.
(43) Ju, Y.; Sun, Y.; Tan, J.; Bu, H.; Han, K.; Li, X.; Fang, L. The composition, pore structure characterization and deformation mechanism of coal-bearing shales from tectonically altered coalfields in eastern China. *Fuel* **2018**, *234*, 626−642.
(44) Zhang, Z.; Qin, Y.; Zhuang, X.; Li, G.; Liu, D. Geological controls on the CBM productivity of No.15 coal seam of Carboniferous−Permian Taiyuan Formation in Southern Qinshui Basin and prediction for CBM high-yield potential regions. *Acta Geol. Sin. - Engl. Ed.* **2018**, *92*, 2310−2332.
(45) Meng, Z.; Yan, J.; Li, G. Controls on gas content and carbon isotopic abundance of methane in Qinnan-East coal bed methane Block, Qinshui Basin, China. *Energy Fuels* **2017**, *31*, 1502−1511.
(46) Yin, L.; Guo, S. Accumulation conditions of tight gas in Shanxi Formation, Qinshui Basin. *Sci. Technol. Eng.* **2020**, *20*, 8057−8065.
(47) Zhao, J.; Sheng, S.; Wang, D.; Lu, J.; Zhang, J.; Liu, G.; Cui, H. Analysis on evolution, modification and hydrocarbon resources potential of the Upper Paleozoic in the Linfen-Yuncheng Basin. *Geol. Rev.* **2019**, *65*, 168−180.
(48) Jasper, K.; Krooss, B. M.; Flajs, G.; Hartkopf-Fröder, C.; Littke, R. Characteristics of type III kerogen in coal-bearing strata from the Pennsylvanian (Upper Carboniferous) in the Ruhr Basin, Western Germany: Comparison of coals, dispersed organic matter, kerogen concentrates and coal−mineral mixtures. *Int. J. Coal Geol.* **2009**, *80*, 1−19.
(49) Yi, J.; Tang, S.; Zhang, S.; Yang, N. Analysis on geochemical characteristics of coal - bearing series in hydrocarbon source rocks Yangqu Block of Qinshui Basin. *Coal Sci. Technol.* **2014**, *42*, 233−236.
(50) Yin, S.; Ding, W.; Hu, Q.; Liu, J.; Mei, Y.; Liu, Z. Hydrocarbon source rock characteristics and favorable hydrocarbon - generating area evaluation of Carboniferous - Permian coal measures strata in Qinshui basin, Shanxi, China. *J. Chengdu Univ. Technol., Sci. Technol. Ed.* **2016**, *43*, 163−176.
(51) Zhao, K.; Fu, X.; Zhang, M.; Cheng, W.; Qu, L. Evaluation of organic geochemical characteristics and hydrocarbon generation potential of coal measure mud shale. *Coal Sci. Technol.* **2019**, *47*, 182−188.
(52) Duan, Y.; Wu, B.; Zheng, C.; Wang, C.; Tao, M. Thermal simulation of gas generation of coal rocks and its significance tracing coalbed methane formation. *Nat. Gas Ind.* **2005**, *25*, 66−69.
(53) Dong, Z.; Zhang, M.; Zhang, J.; Sun, M.; Liu, J.; Qian, Z. Study on thermal simulation experiment of gaseous hydrocarbon generation of Shanxi Formation coal in Qinshui Basin. *J. Anhui Univ. Sci. Technol., Nat. Sci.* **2014**, *34*, 6−11.
(54) Zhang, W.; Li, X. Hydrocarbon generation capacity analysis of main coal measure gas source rocks in China. *Coal Geol. Explor.* **1988**, 31−37.
(55) Dong, Z.; Li, X.; Yang, J.; Sun, J.; Huang, X.; Mi, J.; Wen, Z.; Liu, J. An experimental study on coal measures source rock gas generation thermal simulation. *Coal Geol. China* **2015**, *27*, 12−17.
(56) Liu, X.; Wang, Z.; Pang, X. Numerical simulation of coal-formed gas generating rate for lignite and its geological significance [J]. *Pet. Explor. Dev.* **1996**, *23*, 5−7.
(57) Pang, X.; Chen, Z.; Fang, Z. Mathematical simulation calculation of gas incidence rate. *J. Daqing Pet. Inst.* **1985**, 52−67.

https://doi.org/10.1021/acsomega.1c02211
ACS Omega 2021, 6, 17660−17673

(58) Hou, H.; Shao, L.; Wang, S.; Xiao, Z.; Wang, X.; Li, Z.; Mu, G. Influence of depositional environment on coalbed methane accumulation in the Carboniferous-Permian coal of the Qinshui Basin, northern China. *Front. Earth Sci.* **2019**, *13*, 535−550.
(59) Qin, Y.; Shen, J. On the fundamental issues of deep coalbed methane geology. *Acta Pet. Sin.* **2016**, *37*, 125−136.
(60) Zhao, M.; Song, Y.; Su, X.; Liu, S.; Qin, S.; Hong, F.; Lin, X. The key stage and moment of coalbed gas reservior evolution in the Qinshui Basin, China. *Chin. Sci. Bull.* **2005**, 92−98.
(61) Meng, Y.; Wang, X.; Li, B.; Cai, Z. Thermal evolution history of Qinshui Basin in the middle of North China Cratonand Mesozoic-Cenozoic lithosphere thectonic evolution in Shanxi Plateau. *Northwest. Geol.* **2015**, *48*, 159−168.
(62) Zhao, Z.; Pang, X.; Jiang, F.; Wang, K.; Li, L.; Zhang, K.; Zheng, X. Hydrocarbon generation from confined pyrolysis of lower Permian Shanxi Formation coal and coal measure mudstone in the Shenfu area, northeastern Ordos Basin, China. *Mar. Pet. Geol.* **2018**, *97*, 355−369.
(63) Liu, Q.; Jin, Z.; Meng, Q.; Wu, X.; Jia, H. Genetic types of natural gas and filling patterns in Daniudi gas field, Ordos Basin, China. *J. Asian Earth Sci.* **2015**, *107*, 1−11.
(64) Hanson, A. D.; Ritts, B. D.; Moldowan, J. M. Organic geochemistry of oil and source rock strata of the Ordos Basin, north-central China. *AAPG Bull.* **2007**, *91*, 1273−1293.
(65) Shuai, Y.; Zhang, S.; Mi, J.; Gong, S.; Yuan, X.; Yang, Z.; Liu, J.; Cai, D. Charging time of tight gas in the Upper Paleozoic of the Ordos Basin, central China. *Org. Geochem.* **2013**, *64*, 38−46.
(66) Guoyi, H.; Jin, L.; Xiuqin, S.; Zhongxi, H. The origin of natural gas and the hydrocarbon charging history of the Yulin gas field in the Ordos Basin, China. *Int. J. Coal Geol.* **2010**, *81*, 381−391.
(67) Dai, J.; Li, J.; Luo, X.; Zhang, W.; Hu, G.; Ma, C.; Guo, J.; Ge, S. Stable carbon isotope compositions and source rock geochemistry of the giant gas accumulations in the Ordos Basin, China. *Org. Geochem.* **2005**, *36*, 1617−1635.
(68) Wang, F.; Guo, S. Shale gas content evolution in the Ordos Basin. *Int. J. Coal Geol.* **2019**, 103231.
(69) Yu, K.; Ju, Y.; Qi, Y.; Huang, C.; Zhu, H. Geological process of Late Paleozoic shale gas generation in the eastern Ordos Basin, China: Revelations from geochemistry and basin modeling. *Int. J. Coal Geol.* **2020**, *229*, 103569.
(70) Zhao, X.; Zhou, L.; Pu, X.; Jiang, W.; Jin, F.; Xiao, D.; Han, W.; Zhang, W.; Shi, Z.; Li, Y. Hydrocarbon-generating potential of the Upper Paleozoic section of the Huanghua Depression, Bohai Bay Basin, China. *Energy Fuels* **2018**, *32*, 12351−12364.
(71) Akande, S. O.; Lewan, M. D.; Egenhoff, S.; Adekeye, O.; Ojo, O. J.; Peterhansel, A. Source rock potential of lignite and interbedded coaly shale of the Ogwashi−Asaba Formation, Anambra basin as determined by sequential hydrous pyrolysis. *Int. J. Coal Geol.* **2015**, *150-151*, 224−237.
(72) Bilkiewicz, E.; Kowalski, T. Origin of hydrocarbon and non-hydrocarbon (H2S, CO2 and N2) components of natural gas accumulated in the Zechstein Main Dolomite (Ca2) strata in SW part of the Polish Permian Basin: stable isotope and hydrous pyrolysis studies. *J. Pet. Sci. Eng.* **2020**, *192*, 107296.
(73) Popov, E.; Kalmykov, A.; Cheremisin, A.; Bychkov, A.; Bondarenko, T.; Morozov, N.; Karpov, I. Laboratory investigations of hydrous pyrolysis as ternary enhanced oil recovery method for Bazhenov formation. *J. Pet. Sci. Eng.* **2017**, *156*, 852−857.
(74) Lewan, M. D.; Kotarba, M. J. Thermal-maturity limit for primary thermogenic-gas generation from humic coals as determined by hydrous pyrolysis. *AAPG Bull.* **2014**, *98*, 2581−2610.
(75) Song, H.; Bao, J.; Wen, Z.; Cheng, D. Comparative study of aromatic hydrocarbons in bitumens and expelled oils generated by hydrous pyrolysis of coal. *Int. J. Coal Geol.* **2019**, 103303.
(76) Jin, Q.; Hou, Q.; Cheng, F.; Wang, S.; Zhang, R.; Wang, F. Evaluation method of effective source rock in mature exploration area: a case study of Liaodong Bay. *Acta Pet. Sin.* **2019**, *40*, 257−267.
(77) Takahashi, K. U.; Nakajima, T.; Suzuki, Y.; Morita, S.; Sawaki, T.; Hanamura, Y. Hydrocarbon generation potential and thermal maturity of coal and coaly mudstones from the Eocene Urahoro Group in the Kushiro Coalfield, eastern Hokkaido, Japan. *Int. J. Coal Geol.* **2020**, *217*, 103322.

https://doi.org/10.1021/acsomega.1c02211
ACS Omega 2021, 6, 17660−17673